Astronomy
&
Astrophysics

1RXS J180408.9-342058: An ultra compact X-ray binary candidate with a transient jet[*],[**]

M. C. Baglio[1,2], P. D'Avanzo[2], S. Campana[2], P. Goldoni[3], N. Masetti[4,5], T. Muñoz-Darias[6,7], V. Patiño-Álvarez[8], and V. Chavushyan[8]

[1] Università dell'Insubria, Dipartimento di Scienza e Alta Tecnologia, via Valleggio 11, 22100 Como, Italy
e-mail: cristina.baglio@brera.inaf.it
[2] INAF, Osservatorio Astronomico di Brera, via E. Bianchi 46, 23807 Merate (LC), Italy
[3] APC, Astroparticules et Cosmologie, Université Paris Diderot, CNRS/IN2P3, CEA/Irfu, Observatoire de Paris, Sorbonne Paris Cité, 10 rue Alice Domon et Léonie Duquet, 75205 Paris Cedex 13, France
[4] INAF–Istituto di Astrofisica Spaziale e Fisica Cosmica di Bologna, via Gobetti 101, 40129 Bologna, Italy
[5] Departamento de Ciencias Físicas, Universidad Andrés Bello, Fernández Concha 700, Las Condes, Santiago, Chile
[6] Instituto de Astrofisica de Canarias, 38205 La Laguna, Tenerife, Spain
[7] Departamento de astrofisica, Universidad de La Laguna, 38206 La Laguna, Tenerife, Spain
[8] Instituto Nacional de Astrofísica, Óptica y Electrónica, Apartado Postal 51-216, 72000 Puebla, Mexico

ABSTRACT

Aims. We present a detailed near-infrared/optical/UV study of the transient low-mass X-ray binary 1RXS J180408.9-342058 performed during its 2015 outburst, which is aimed at determining the nature of its companion star.
Methods. We obtained three optical spectra ($R \sim 1000$) at the 2.1 m San Pedro Mártir Observatory telescope (México). We performed optical and NIR photometric observations with both the REM telescope and the New Technology Telescope (NTT) in La Silla. We obtained optical and UV observations from the *Swift* archive. Finally, we performed optical polarimetry of the source using the EFOSC2 instrument mounted on the NTT.
Results. The optical spectrum of the source is almost featureless since the hydrogen and He I emissions lines, typically observed in LMXBs, are not detected. Similarly, carbon and oxygen lines are not observed either. We marginally detect the He II 4686 Å emission line, suggesting the presence of helium in the accretion disc. No significant optical polarisation level was observed.
Conclusions. The lack of hydrogen and He I emission lines in the spectrum implies that the companion is likely not a main-sequence star. Driven by the tentative detection of the He II 4686 Å emission line, we suggest that the system could harbour a helium white dwarf. If this is the case, 1RXS J180408.9-342058 would be an ultra-compact X-ray binary. By combining an estimate of the mass accretion rate together with evolutionary tracks for a He white dwarf, we obtain a tentative orbital period of ~40 min. We also built the NIR-optical-UV spectral energy distribution (SED) of the source at two different epochs. One SED was gathered when the source was in the soft X-ray state and this SED is consistent with the presence of a single thermal component. The second SED, obtained when the source was in the hard X-ray state, shows a thermal component along with a tail in the NIR, which likely indicates the presence of a (transient) jet.

Key words. X-rays: binaries – stars: neutron – stars: jets

1. Introduction

Low-mass X-ray binaries (LMXBs) are accreting binary systems hosting a compact object (either a stellar massive black hole or a neutron star) and a companion star that is usually a main-sequence, low-mass star. In such systems the transfer of mass takes place via Roche lobe overflow and the consequent formation of an accretion disc around the compact object. Depending on the nature of the companion star, LMXBs usually have orbital periods varying from minutes to days. In particular, a class of tight LMXBs exists that is called ultra-compact X-ray binaries (UCXBs), which are characterised by orbital periods <80 min

and usually harbour white dwarfs or hydrogen-poor stars as companions.

The nature of LMXBs can be both transient or persistent. The former group alternate between short (weeks–months) and sudden periods of outburst, characterised by a typical X-ray luminosity of $10^{36}-10^{38}$ erg/s, during which the compact object accretes at high rates, to long lasting (years to decades) periods of quiescence, when the X-ray luminosity drops up to seven orders of magnitude.

The X-ray source 1RXS J180408.9-342058 (hereafter J180408) was first identified as a neutron star (NS) LMXB after the INTEGRAL detection of a type I thermonuclear burst in 2012 (Chenevez et al. 2012). Assuming the Eddington luminosity as an upper limit, Chenevez et al. (2012) limited the distance of this source to 5.8 kpc. Since then, the source remained in quiescence until Jan. 22, 2015, when the *Swift*/BAT detected a new outburst (Krimm et al. 2015a). This outburst was characterised by a slow rise without the detection

---

Table 1. Complete log and results of the NTT observations performed on Feb. 8, 2015.

Filter	Exposures (s)	UT mid observation YYYYmmdd (MJD)	Wavelength (Å)	Mean Magnitude	A_λ (mag)	χ^2/d.o.f.
B	8×15	20150208.3735 (57061.3735)	4400	18.03 ± 0.03	1.73 ± 0.12	15.41/4
V	8×15	20150208.3708 (57061.3708)	5476	17.71 ± 0.02	1.30 ± 0.09	52.63/7
R	8×15	20150208.3614 (57061.3614)	6431	17.24 ± 0.03	1.04 ± 0.07	2.7/4
i	8×15	20150208.3661 (57061.3661)	7931	17.03 ± 0.06	0.75 ± 0.05	6.389/7

Notes. The magnitude values (Vega) are not corrected for reddening, which is reported in the 6th column (Schlafly & Finkbeiner 2011). In the last column, the χ^2/d.o.f. of the constant fits performed on the light curves are reported. Errors are indicated at a 90% c.l.

of Type I bursts. A MAXI/GSC X-ray spectrum on Jan. 26−28, 2015 showed a hard spectrum, which can be modelled by a power law with an index 1.68 ± 0.27 (Negoro et al. 2015). Since the detection of the outburst, the source was regularly monitored by *Swift*. In particular, Krimm et al. (2015b) reported an increase in brightness in the hard X-ray band (15−50 keV) after the first 20 days of activity, which then plateaued at an average rate of ~100 mCrab. Radio observations obtained with the VLA and contemporaneous *Swift* X-ray observations showed that the position of the source in the radio/X-ray luminosity plane was consistent with that of hard-state neutron star LMXBs (Deller et al. 2015). While the source was in its hard state, radio emission consistent with jets was also detected in the radio band (Deller et al. 2015; Degenaar et al. 2015).

Around Apr. 3, 2015, a significant drop in the hard X-ray flux was detected with an increase in the softer X−rays (2−10 keV), suggesting that the source transitioned to a soft X-ray spectral state (Degenaar et al. 2015).

2. Observation and data analysis

2.1. Optical spectroscopy

The system J180408 was observed on Apr. 20, 2015 with the 2.1 m telescope at the San Pedro Mártir Observatory (México), equipped with the Boller & Chivens spectrograph. Three 1800 s spectra with a resolution of ~6.5 Å (350 km s^{-1}) were acquired, covering the wavelength range 4000−7800 Å. The three spectra were combined and averaged to obtain one final spectrum to increase the signal to noise ratio (S/N).

Data reduction was carried out using standard procedures for both bias subtraction and flat-field correction with IRAF[1]. The wavelength calibration was carried out with neon-helium-copper-argon lamps. The flux calibration was performed against the catalogued spectroscopic standard star Feige 67 (Massey et al. 1988).

2.2. New Technology Telescope (NTT) photometry

The LMXB J180408 was observed at the La Silla observatory with the New Technology Telescope (NTT) on Feb. 8, 2015 using the instrument EFOSC2 equipped with the optical Bessel *BVR* and Gunn *i* filters (4400−7930 Å). A total of 8×15 s images for each filter was obtained in each band. A log of the observations is reported in Table 1.

Bias and flat-field corrections have been applied with the standard procedures: subtraction of an average bias frame and division by a normalised average flat field. Because of the crowdedness of the field, all the magnitudes were extracted performing

point spread function (PSF) photometry with the ESO MIDAS[2] `daophot` task (Stetson 1987). The night was clear with seeing ~0.7−0.8″ for the whole duration of the observation. We performed differential photometry with respect to a selection of 14 isolated stars in the field.

2.3. Rapid Eye Mount (REM) observations

J180408 was observed in the optical (SDSS *griz* filters simultaneously) and NIR (2MASS *JK*-bands, one filter at a time) with the REM telescope (Zerbi et al. 2001; Covino et al. 2004) on 2015 Feb. 26, 2015 and Apr. 24, 2015, i.e. before and soon after the change of its X-ray state from hard to soft (Degenaar et al. 2015). A complete log of the observations is reported in Table 2.

Each image was bias and flat-field corrected using standard procedures, and PSF photometry techniques were applied to obtain the magnitudes of all the objects in the field. Both nights were clear and seeing remained constant during the whole duration of the observations. We performed differential photometry with respect to a selection of the same six bright and isolated stars of the field to correct for any instrumental effect. The target is well detected in the *gri* filters, but not in the *z*-band, which was excluded from the analysis.

The calibration of the optical photometry (NTT and REM) was performed through the comparison between the fluxes measured for a group of isolated stars in the fields, chosen as reference with the fluxes tabulated in the APASS[3] catalogue (Sect. 2.3). We applied the corrections reported in Jordi et al. (2006) for the NTT observations to pass from the *gri* magnitudes, i.e. the SDSS filters used in the APASS catalogue, to the *BVR* magnitudes (Johnson filters, used in EFOSC2)

2.4. Swift/UVOT observations

After the onset of the outburst, the system J180408 has been extensively observed both in X-rays and UV frequencies by the *Swift* satellite. In particular, we analysed the UVOT data from the observations that started on 2015 Feb. 26, 2015 because this was contemporaneous to the first set of REM observations. A complete log of the UVOT observations is reported in Table 3.

We performed the analysis of the data via the HEASOFT routine *uvotsource* after we defined the extraction region, which is a circle centred on the source with a radius of 4 arcsec, and the background, which is a circle with radius of 9.5 arcsec.

---

[1] http://iraf.noao.edu/

[2] http://www.eso.org/sci/software/esomidas/
[3] http://www.aavso.org/download-apass-data

Table 2. Complete log and results of the REM observations in the two epochs (Feb. 26, 2015 and Apr. 24, 2015).

Filter	Exposures (s)	UT mid observation YYYYmmdd (MJD)	Wavelength (Å)	Mean Magnitude	A_λ (mag)	χ^2/d.o.f.
2015 February 26						
g	32×30	20150226.3423 (57079.3423)	4770	17.84 ± 0.05	1.56 ± 0.06	58.3/30
r	32×30	20150226.3423 (57079.3423)	6231	17.38 ± 0.03	1.06 ± 0.04	78.4/27
i	32×30	20150226.3423 (57079.3423)	7625	17.02 ± 0.03	0.75 ± 0.03	42.9/31
J	22×15	20150226.3394 (57079.3394)	12 350	15.79 ± 0.12	0.33 ± 0.01	–
K	4×15	20150226.3309 (57079.3309)	21 590	14.68 ± 0.26	0.14 ± 0.01	–
2015 April 24						
g	12×30	20150424.2584 (57136.2584)	4770	17.02 ± 0.04	1.56 ± 0.06	5.3/11
r	12×30	20150424.2584 (57136.2584)	6231	16.78 ± 0.03	1.06 ± 0.04	12.9/11
i	12×30	20150424.2584 (57136.2584)	7625	17.08 ± 0.03	0.75 ± 0.03	28.2/11
J	8×15	20150424.2437 (57136.2437)	12 350	16.84 ± 0.16	0.33 ± 0.01	–

Notes. The magnitude values (AB magnitudes) are not corrected for reddening; the parameters for these values are in the 6th column (Schlafly & Finkbeiner 2011). In the last column, the χ^2/d.o.f. of the constant fits performed (where possible) on the light curves are reported. Errors are indicated at a 90% c.l.

Table 3. Complete log and results of the *Swift*/UVOT observations taken on Feb. 26, 2015.

Filter	Exposure time (s)	UT mid observation YYYYmmdd (MJD)	Wavelength (Å)	Magnitude	A_λ (mag)
b	122	20150226.1099 (57079.1099)	4392	17.22 ± 0.08	1.66 ± 0.06
u	122	20150226.1088 (57079.1088)	3465	16.45 ± 0.06	2.01 ± 0.07
$w1$	244	20150226.2133 (57079.2133)	2600	16.90 ± 0.07	2.69 ± 0.10
$m2$	322	20150226.1203 (57079.1203)	2246	17.86 ± 0.12	3.73 ± 0.14
$w2$	488	20150226.1140 (57079.1140)	1928	17.58 ± 0.08	3.31 ± 0.12

Notes. The (Vega) magnitudes are not corrected for reddening. The parameters of the reddening are reported in the last column (Schlafly & Finkbeiner 2011). Errors are indicated at a 90% c.l. *v* data were not used due the simultaneous occurrence of a Type I burst.

Table 4. Complete log and results (3σ upper limits) of the NTT polarimetric observations taken on Feb. 9, 2015.

Filter	Exposure time per pos. angle (s)	UT mid observation YYYYmmdd (MJD)	3σ upper limit
B	160	20150209.3670 (57062.3670)	<6.9%
V	120	20150209.3589 (57062.3589)	<5.6%
R	120	20150209.3414 (57062.3414)	<1.4%
i	180	20150209.3498 (57062.3498)	<1.6%

2.5. Optical polarimetry with NTT

J180408 was observed on 2015 Feb. 9, 2015 with the optical polarimeter of EFOSC2, mounted on the NTT, equipped with the *BVRi* filters. The night was clear: seeing ~0.7″ during the whole duration of the observation. Image reduction was carried out by bias subtraction and division by a normalised flat-field. A complete log of the observation is presented in Table 4. We performed all the flux measurements via the technique of PSF photometry (as explained in Sect. 3.2.1).

A Wollaston prism was inserted in the optical path, so that incident radiation was simultaneously split into two different beams with orthogonal polarisation (ordinary and extraordinary beams, *o*- and *e*-beams). Furthermore, a Wollaston mask prevented the possible overlap of the different images. The instrument made use of a rotating half-wave plate (HWP) to take images at four different angles with respect to the telescope axis ($\Phi_i = 22.5°(i-1)$, $i = 0, 1, 2, 3$). One image of 15 s integration was obtained for each HWP angle for the *BVRi* filters.

3. Results

3.1. Optical spectroscopy

The flux-calibrated, barycentric-corrected, and co-added spectrum is shown in Fig. 1. We detected absorption features from the Galactic sodium doublet at 5890 Å and the MgIb band at 5175 Å. The spectrum does not show prominent emission lines at variance with LMXBs in outburst. In Fig. 1, we indicate the most common hydrogen emission lines (H_α at 6563 Å and H_β at 4861 Å), whereas the positions of the most prominent He I emission lines are shown with dashed lines (4713, 4921, 5015, 5876, and 6678 Å) and none is detected. On the contrary, we observe the presence of an emission feature at $\lambda = 4686.3 \pm 1.5$ Å, which could correspond to the 4686 Å He II (see dotted line in Fig. 1). According to an F-test, the fit of this line with a Gaussian function is preferable to that with a constant at a ~4σ significance over the 4670–4705 Å range). This seems to suggest that a certain quantity of helium may be present in the accretion disc of the system. For this possible emission line, we derived an equivalent width (EW) of 1.5 ± 0.2 Å and a systemic velocity of 19.2 ± 96.1 km s^{-1}.

3.2. Near-infrared/optical/UV photometry

3.2.1. Optical observations with NTT

The results of the NTT *BVRi* photometry performed on Feb. 8, 2015 (MJD 57 061) are reported in Table 1. The optical counterpart of J180408 is well detected in each image (Bessel *BVR*
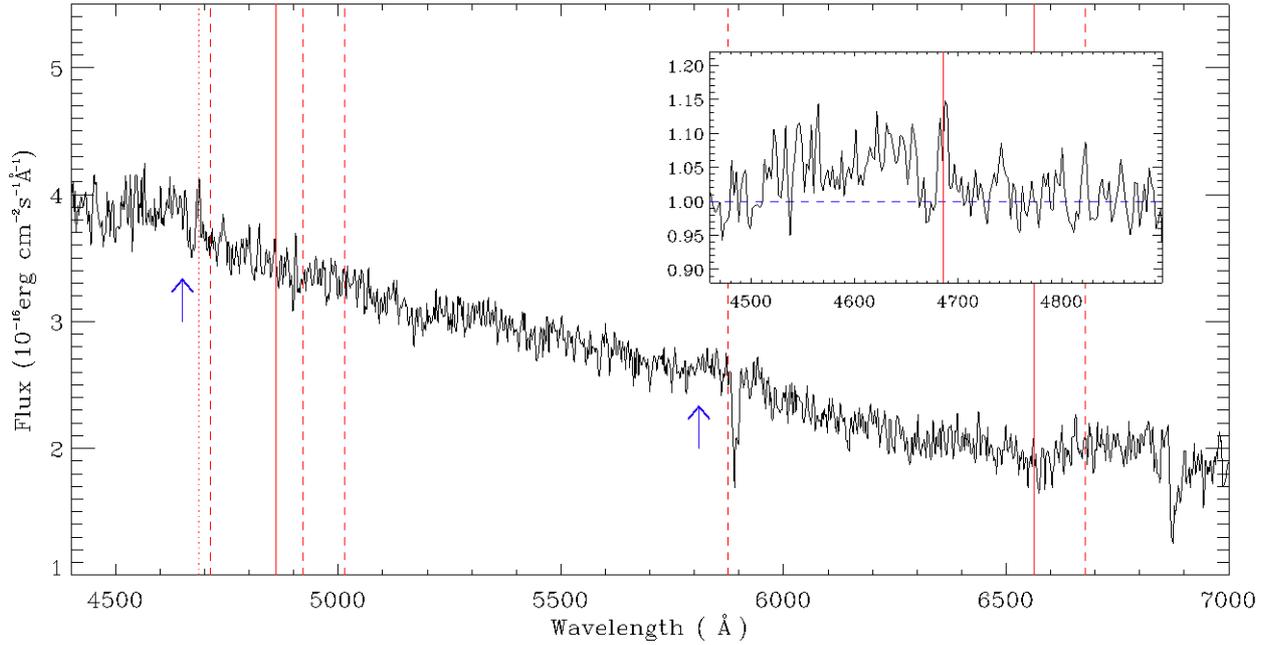
Fig. 1. Averaged, flux-calibrated spectrum of J180408 obtained at the San Pedro Mártir Observatory (Mexico) on Apr. 20, 2015 (MJD 57 132). The spectrum is not corrected for reddening. Solid lines indicate the positions of the most common hydrogen lines ($H_\alpha = 6563$ Å and $H_\beta = 4861$ Å); dashed lines indicate the most prominent He I emission line positions (4713, 4921, 5015, 5876 and 6678 Å); finally, a dotted line indicates the wavelength of the He II line at 4686 Å. Two blue arrows indicate the tabulated position of the two suggested carbon lines (C II 4650 Å and C III 5810 Å). *Inset*: a zoom of the spectrum centred on the possibly detected He II line after the normalisation of the spectrum continuum to 1 is represented. A solid line indicates the position of the He II line (4686 Å).
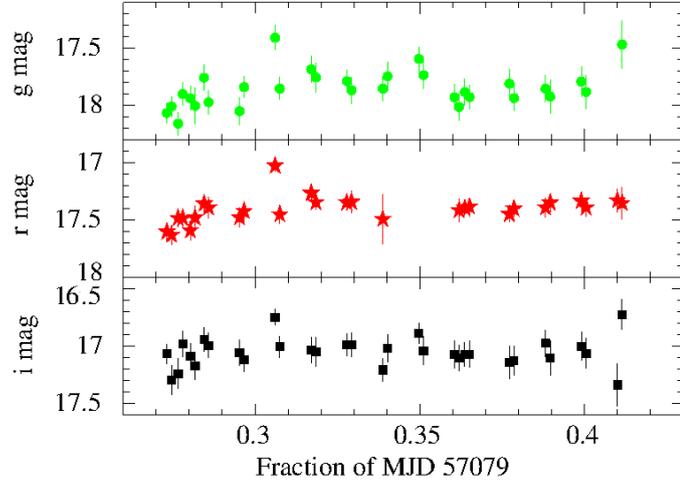

Fig. 2. *From top to bottom*, *g, r, i* light curves for the system J180408 observed with REM on Feb. 26, 2015. Errors are indicated at the 68% confidence level.
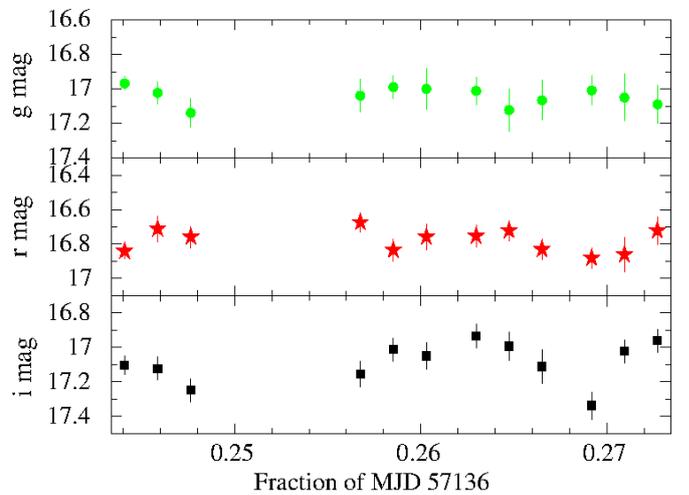

Fig. 3. *From top to bottom*, *gri* light curves obtained with the REM telescope on Apr. 24, 2015. Errors are indicated at the 68% confidence level.

and Gunn *i*). The source shows a clear intrinsic variability in all bands, even on a relatively short timescale (minutes). As shown in Table 1, the fit of the light curves with a constant function gives as a result values of χ^2/d.o.f. that prove the low significance of the fit because of the high erratic variability of the source.

3.2.2. Observations with REM

The *gri* light curves of J180408 obtained with the REM telescope on 2015 Feb. 26, 2015 (MJD 57 079, before the state

change) are shown in Fig. 2. The source shows intrinsic variability even at this epoch of observation, resulting in high values of χ^2/d.o.f. in case of a constant fit (Table 2). Similar conclusions can be deducted from the light curves obtained for J180408 on 2015 Apr. 24, 2015 (MJD 57 136, Fig. 3), i.e. soon after the transition from the hard to soft X-ray state. Table 2 lists the mean magnitudes obtained in the *g, r, i*-bands from the fit of the light curves with a constant. In the NIR, in contrast to the optical observations, we do not possess enough data to build light curves. Thus, we averaged all the images to derive the infrared magnitudes reported in Table 2.

3.2.3. Observations with Swift/UVOT

J180408 was observed by the *Swift* satellite on Feb. 26, 2015 (MJD 57 079, Table 3). *Swift*/UVOT observed with all its filters, however, because of the contemporaneous detection of a Type-I burst, the *v*-band image has been excluded from the analysis. The calibrated magnitudes of the target (obtained as described in Sect. 2.4) and the absorption coefficients for each filter (Schlafly & Finkbeiner 2011) are reported in Table 3.

3.3. Optical polarimetry with the NTT

With the aim of evaluating the degree of linear polarisation P of the system, for each value of the instrumental position angle Φ, we computed the quantity

$$S(\Phi) = \left(\frac{f^\circ(\Phi)/f^e(\Phi)}{\langle f^\circ_u(\Phi)/f^e_u(\Phi_i) \rangle} - 1 \right) \bigg/ \left(\frac{f^\circ(\Phi)/f^e(\Phi)}{\langle f^\circ_u(\Phi)/f^e_u(\Phi) \rangle} + 1 \right), \quad (1)$$

where f°, f^e are the fluxes in the ordinary and extraordinary beams and $\langle f^\circ_u(\Phi)/f^e_u(\Phi) \rangle$ is the averaged ratio between the ordinary and extraordinary fluxes of the unpolarised field stars that we chose as reference stars. As exhaustively described in di Serego Alighieri (1998), this parameter gives an estimate of the projection of the polarisation along the different directions. The parameters S and the polarisation degree and angle (P and θ_P, respectively) are then related through the relation

$$S(\Phi) = P \cos 2(\theta - \Phi). \quad (2)$$

The fit of $S(\Phi)$ with Eq. (2) returns P from the semi-amplitude of the oscillation and θ_P from the position of the first maximum of the curve. This method makes any additional correction (interstellar and instrumental effects) unnecessary, since S is already normalised to the non-polarised reference stars. The polarisation degrees are consistent with zero in all bands. We derived 3σ upper limits to the optical polarisation of the target, which are quoted in Table 4. Except for the B and V-bands, the upper limits obtained are lower than the expected maximum interstellar contribution to the LP of 3.9%, evaluated following Serkowski et al. (1975).

4. Discussion

4.1. A possible ultra-compact nature for J180408

The apparent absence of H and He I lines is uncommon for typical LMXBs that harbour a main-sequence companion star. LMXBs may also host a degenerate companion, such as a white dwarf or a hydrogen-poor star. In this case, the orbital period should be short to fill the Roche lobe, and these LMXBs belong to the UCXBs class. Nelemans et al. (2004) analysed the spectra of three UCXBs (4U 0614+091, 4U 1543-624, and 2S 0918-549). Hydrogen and He I emission lines were not detected in any of these, as for J180408. The case of 4U 0614+091 was particularly intriguing since its spectrum shows prominent emission lines that could not be connected to hydrogen and helium lines. Instead, they were consistently identified with carbon and oxygen lines, leading to the conclusion that the companion star was a carbon-oxygen (CO) WD. Similar conclusions were also deducted for the other UCXBs reported in Nelemans et al. (2004).

As described in Sect. 3.1, the spectrum of J180408 is rather featureless, except for the possible detection of a weak He II 4686 Å line, suggesting that helium is present in the accretion disc of the system. However, the total absence of H and He I lines is unusual and reminiscent of the behaviour of UCXBs. We thus compared the spectrum of 4U 0614+091 with that of J180408, aiming to identify possible carbon and oxygen emission lines in the spectrum of our target. Despite the moderate S/N of the spectrum (Fig. 1), no clear evidence for C/O lines can be derived. We only find hints of two possible emission lines, C II 4650 Å and the C III 5810 Å, which correspond to those lines listed in Nelemans et al. (2004) and Baglio et al. (2014). The C II 4650 Å line may be confused with the so-called Bowen blend, which is usually observed in LMXBs, owing to a fluorescence mechanism driven by helium that principally results in the emission of NIII 4634/4640 Å and CIII 4647/4650 Å lines from the strongly irradiated face of the companion star. A possible feature consistent with the Bowen blend is present in our spectrum or even a P-Cygni profile for the weak He II 4686 Å line, but we consider them of too low S/N to lead us to firm conclusions.

The best way to assess whether a LMXB is a UCXB is to measure its orbital period. To this aim we analysed the optical light curves that we obtained with REM both in February 2015 (covering ~3.4 h; Fig. 2) and April 2015 (covering ~0.7 h; Fig. 3), but we found no evidence for a periodicity, only erratic variability. This erratic variability is typical of LMXBs during an outburst, and it hampers photometric studies, especially for UCXBs (Nelemans et al. 2004; Baglio et al. 2014). We thus tried to constrain the orbital period of the system in an alternative way. Starting from the hypothesis of the ultra-compact nature of J180408, we evaluated its mass accretion rate $\dot{M}$. To do this, we considered the MAXI and the RXTE light curves in the $2-10$ and $2-20$ keV band (respectively) and we integrated the counts of J180408 over the duration of the 2015 outburst. Since no other significant outburst occurred since the first detection of the system, we averaged our luminosity over the total time of the MAXI (first) and the RXTE+MAXI monitoring, obtaining $\dot{M} = 4.0 \times 10^{-11}\, M_\odot/\text{yr}$ and $\dot{M} = 1.2 \times 10^{-11}\, M_\odot/\text{yr}$, respectively; a Crab-like spectrum has been assumed for this conversion. We also point out that the short X-ray burst that took place in 2012 (Chenevez et al. 2012) produces only a minimal change to the estimate of the mean accretion rate above. The transient behaviour in LMXBs is usually explained in terms of accretion disc instabilities (DIM model; Lasota et al. 2008). A LMXB should have a mean mass accretion rate below a critical rate to exhibit outbursts. For a He donor star (and orbital periods lower than 60 min) this implies a loose limit on the mass accretion rate of below $\lesssim 10^{-10}\, M_\odot/\text{yr}$ (Lasota et al. 2008). In addition, if we consider that the evolutionary track of a He donor in a UCXB matches our mass accretion rate for J180408, we can derive an estimate for the orbital period. Based on the tracks presented in Lasota et al. (2008, their Fig. 3), we can infer an orbital period around 40 min for J180408. This is clearly an indirect inference and should be confirmed with observations.

4.2. Spectral energy distribution

The system J180408 was observed almost simultaneously (within 5 h) by REM (Table 2) and *Swift*/UVOT (Table 3) on Feb. 26, 2015 (MJD 57 079). This allowed us to build a nearly simultaneous spectral energy distribution (SED) from the NIR to the UV wavelengths. The REM optical (NIR) fluxes were obtained starting from the AB (Vega) magnitudes reported in Table 2, corrected for the reddening due to the Galactic extinction in the direction of the target ($E(B - V) = 0.41$, $A_V/E(B - V) = 3.1$; Schlafly & Finkbeiner 2011). The UV and optical
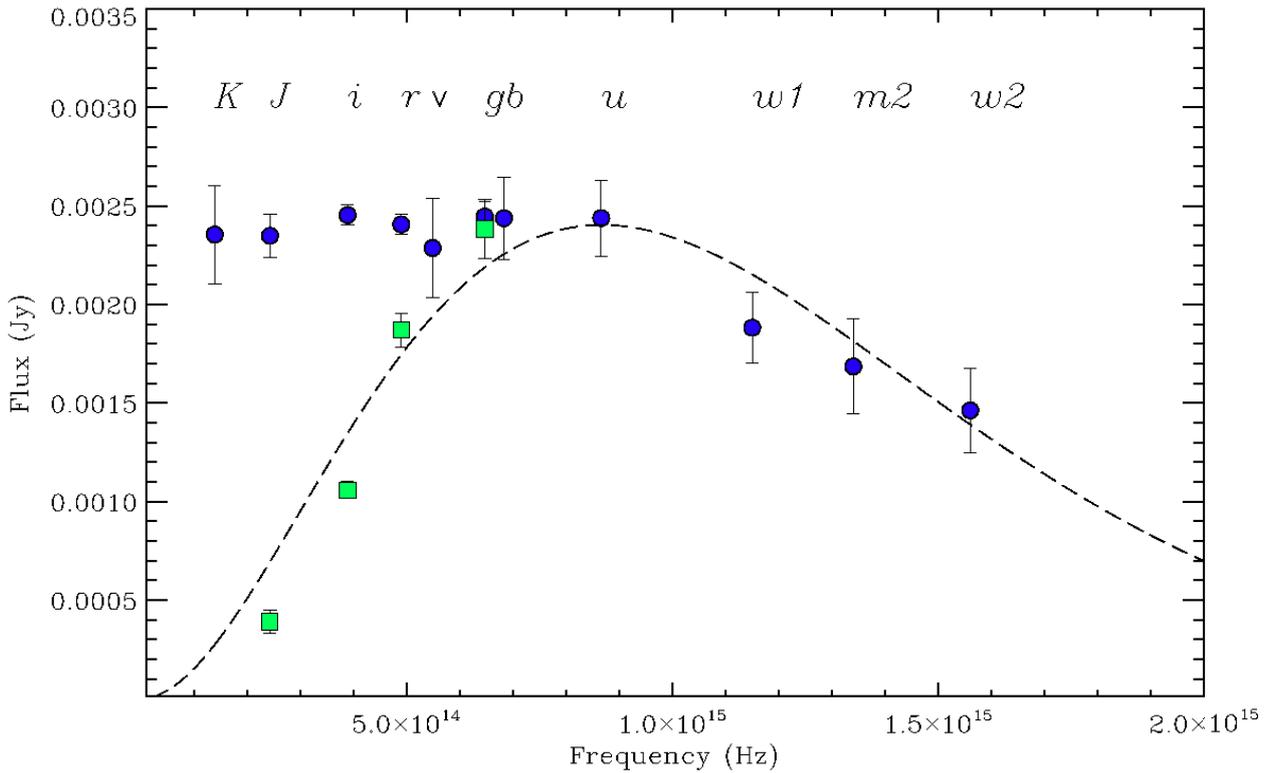
Fig. 4. Spectral energy distributions in the NIR-optical-UV of J180408 relative to the two epochs of Feb. 26, 2015 (MJD 57 079) and Apr. 24, 2015 (MJD 57 136). Green squares depict the *J*-, *i*-, *r*-, *g*-band observations obtained with the REM telescope on Apr. 24; blue dots represent the points relative to the UVOT observations of Feb. 26 and the *K*-, *J*-, *i*-, *r*, *g*-band REM observations taken on Feb. 26.

fluxes relative to the *Swift*/UVOT observations were evaluated from the magnitudes of the target returned by HEASOFT (as described in Sect. 2.4) and reported in Table 3, after correcting for the interstellar absorption.

We applied the same analysis to the second epoch of observations (Apr. 24, 2015 – MJD 57 136), for which we possess the REM infrared and optical photometry (Sect. 3.2.2). In the *K* and *H*-bands the target was too faint to be detected and *Swift* did not observe the system on that occasion.

The NIR-optical-UV SEDs of the two different epochs are represented in Fig. 4. We applied a rigid shift of 1.33 mJy, which corresponds to a factor of ∼2, to all the REM fluxes of the Feb. 26 epoch to be consistent with UVOT fluxes at the same wavelengths.

We focused first on the Feb. 26 epoch and we looked at the highest frequency points (*V* filter onward) in Fig. 4 (blue dots). A fit with an accretion disc model (irradiated or not) does not provide an adequate description of the data. A fit with a black-body model instead provides an acceptable fit (χ^2/d.o.f. = 1.3, 30% null hypothesis probability) with a surface temperature of ∼14 200 K (dashed line in Fig. 4). This black-body emission may come from the hot spot in the stream-disc collision region, companion star, or outer disc regions. The extrapolation of the black-body spectrum largely misses the observations at lower frequency (*r*, *i*, *J*, *K*-bands). This allowed us to hypothesise that the emission process dominating the red part of the SED is different from the one responsible for the blue part of the SED. The flat low-frequency spectrum is highly suggestive of a particle jet emitted from the central regions of the system.

As a result of the small frequency coverage of the second epoch SED (Apr. 24, 2015; green squares in Fig. 4), it was not possible to let the fit with a black body converge to reasonable values, since the peak of the black body was unconstrained. However, the Apr. 24 SED seems to follow the same black body as the Feb. 26 (the dashed line in Fig. 4) somewhat well. This indicates that the putative jet is a transient feature in the SED of J180408.

The presence of jets in LMXBs is usually associated with a hard X-ray spectrum. In the radio band steady jets observed to date during the hard X-ray states have a flat spectrum (e.g. Fender 2001). Above certain frequencies this flat spectral component should break to an optically thin spectrum. There is evidence both from black hole and neutron star X-ray binaries that this break usually occurs in the NIR (Migliari et al. 2010; Gandhi et al. 2011). During its outburst J180408 was monitored by several all-sky instruments, allowing us to trace its spectral evolution (see Fig. 5). As often happens in LMXB outbursts, J180408 started as a hard X-ray source and remained in the so-called hard state for about two months. This is testified by the detection of J180408 with the *Swift*/BAT hard X-ray telescope and the weak detection with the MAXI low-energy monitoring instrument (see e.g. Negoro et al. 2015 and Fig. 5). On Apr. 3, 2015 (MJD 57 115) a drop in the hard X-rays was observed (Degenaar et al. 2015), suggesting that the source transitioned to a soft X-ray spectral state (Fig. 5). Consistently, the MAXI flux was raised considerably.

Our first SED was taken in the hard X-ray state. As described above, this SED shows a flat low-frequency tail, suggestive of a jet. The contribution of the jet seems to be not just restricted to
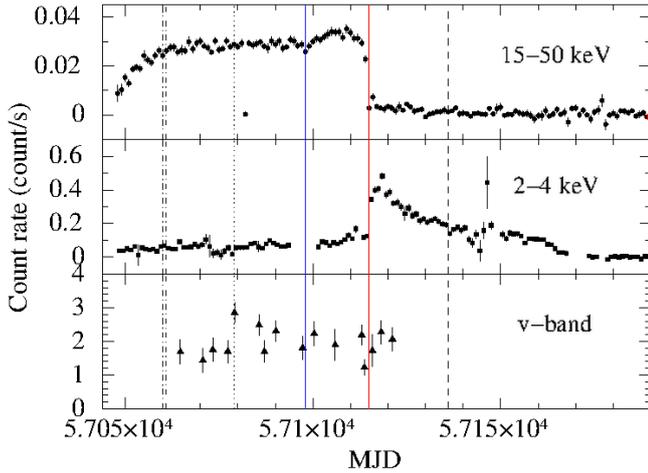
Fig. 5. *From top to bottom*, the monitoring of the system J180408 with the BAT instrument mounted on *Swift* (15−50 keV), the MAXI camera (2−4 keV), and with UVOT (*v*-band) during its outburst, starting from MJD 57 048 (Jan. 26, 2015). The time of the detection of the radio jet (Deller et al. 2015) and the time of the switch to a soft X-ray spectral state are indicated with two solid lines (blue and red, respectively). Dotted and dashed lines indicate the two epochs of our REM observations (Feb. 26−Apr. 24, 2015). Two dot-dashed lines indicate the times of the NTT photometric and polarimetric observations (Feb. 7, 8, 2015).

the NIR spectrum, but appears to be important at least until the *r*-band frequency is reached. The second SED was taken when J180408 was in the soft X-ray state where a steady jet is expected to be quenched, thus explaining the different shapes of the two SEDs (e.g. Russell et al. 2011b; Muñoz-Darias et al. 2014).

In this scenario, the non-detection of linear polarisation when the source was in the hard X-ray state (Sect. 3.3) seems to be puzzling. In fact we would expect to detect some polarised emission at least at a few percent level in the optical-NIR bands (Russell et al. 2011a), if a jet was present. Our polarisation data were collected on Feb. 9, which is some weeks before our likely detection of a jet (Feb. 26). Even if we cannot build a wide band SED, our NTT data collected on Feb. 8 (*BVRi*) are consistent with the low-frequency tail of a black body, as in the case of the second epoch observations with REM, when the jet was not detectable in the SED. We also note that at the time of the polarisation observations, the plateau that corresponds to the hard X-ray spectral state phase of the source (namely when the jet should first arise) was not yet completely reached (and the optical flux was a factor of ~2 lower). We can thus infer that the jet was probably not yet formed at the time of our polarimetric observations or, at least, it might not contribute substantially at optical (*BVRi*) frequencies.

5. Conclusions

In this work we performed a detailed NIR/optical and UV study of the LMXB 1RXS J180408.9-342058. Our principal results are summarised below.

- We observed the optical spectrum during outburst with the aim of identifying the nature of its companion star. The spectrum is rather featureless with no Hα and He I emission lines. This is uncommon for bright LMXBs. We only

marginally detected the He II 4684 Å emission line, suggesting the presence of helium. The lack of hydrogen leads us to hypothesise that the companion star could be a He white dwarf and J180408 be part of the UCXB class.
- We searched our photometric data for an orbital period. No evidence for a periodicity was found. Integrating the long-term, X-ray light curve from all-sky monitoring instruments, we evaluated the mean mass accretion rate of the system. Based on the disc instability model (Lasota et al. 2008) and the evolutionary track for a He white dwarf companion, we estimated the orbital period of J180408 to be ~40 min, which is typical of a UCXB. This inference clearly needs to be verified observationally.
- We built the quasi-simultaneous SED from NIR to UV during the hard X-ray state. We interpret the SED as due to the emission of two components: a black body and a steady jet that emits synchrotron radiation up to the *R*-band. We also built the NIR/optical SED after the transition to a soft X-ray spectral state. As expected, during this epoch the jet seems to be quenched, leaving the black body contribution alone in the SED.
- We did not observe significant polarisation in the optical bands, even though J180408 was in the hard X-ray state. However, at the time of our polarimetric observation, which occurred weeks before our likely detection of the jet in the SED, the hard X-ray state was not completely reached by the source. We conclude that at that time the jet probably was not yet formed or could have been contributing only at lower frequencies, i.e. in the radio band.

References

Baglio, M. C., Mainetti, D., D'Avanzo, P., et al. 2014, A&A, 572, A99
Chenevez, J., Kuulkers, E., Brandt, S., et al. 2012, ATel, 4050, 1
Covino, S., Stefanon, M., Sciuto, G., et al. 2004, SPIE, 5492, 1613
Degenaar, N., Altamirano, D., Deller, A., et al. 2015, ATel, 7352, 1
Deller, A., Degenaar, N., Hessels, J., et al. 2015, ATel, 7255, 1
di Serego Alighieri, S. 1998, Instrumentation for Large Telescopes (Cambridge University Press), 199, 287
Fender, R. P. 2001, MNRAS, 322, 31
Gandhi, P., Blain, A. W., Russell, D. M., et al. 2011, ApJ, 740, L13
Jordi, K., Grebel, E. K., & Ammon, K. 2006, A&A, 460, 339
Krimm, H. A., Barthelmy, S. D., Baumgartner, W., et al. 2015a, ATel, 6997, 1
Krimm, H. A., Kennea, J. A., Siegel, M. H., & Sbarufatti, B. 2015b, ATel, 7039, 1
Lasota, J.-P., Dubus, G., & Kruk, K. 2008, A&A, 486, 523
Massey, P., Strobel, K., Barnes, J. V., & Anderson, E. 1988, ApJ, 328, 315
Migliari, S., Tomsick, J. A., Miller-Jones, J. C. A., et al. 2010, ApJ, 710, 117
Muñoz-Darias, T., Fender, R. P., Motta, S. E., & Belloni, T. M. 2014, MNRAS, 443, 3270
Negoro, H., Sugimoto, J., Mihara, T., et al. 2015, ATel, 7008
Nelemans, G., Jonker, P. G., Marsh, T. R., & van der Klis, M. 2004, MNRAS, 348, L7
Russell, D. M., Casella, P., Fender, R., et al. 2011a, ArXiv eprints [arXiv:1104.0837]
Russell, D. M., Miller-Jones, J. C. A., Maccarone, T. J., et al. 2011b, ApJ, 739, L19
Schlafly, E. F., & Finkbeiner, D. P. 2011, ApJ, 737, 103
Serkowski, K., Mathewson, D. S., & Ford, V. L. 1975, ApJ, 196, 261
Stetson, P. B. 1987, PASP, 99, 191
Zerbi, R. M., Chincarini, G., Ghisellini, G., et al. 2001, Astron. Nachr., 322, 275